JACS
JOURNAL OF THE AMERICAN CHEMICAL SOCIETY
Article
pubs.acs.org/JACS

Formation of [4Fe-4S] Clusters in the Mitochondrial Iron–Sulfur Cluster Assembly Machinery

Diego Brancaccio,[†] Angelo Gallo,[‡,§] Maciej Mikolajczyk,[‡,§] Kairit Zovo,[∥] Peep Palumaa,[∥] Ettore Novellino,[†] Mario Piccioli,[‡,§] Simone Ciofi-Baffoni,[‡,§] and Lucia Banci*[,‡,§]

[†]Department of Pharmacy, University of Naples "Federico II", Via D. Montesano 49, 80131 Napoli, Italy
[‡]Department of Chemistry, University of Florence, Via della Lastruccia 3, 50019 Sesto Fiorentino, Florence, Italy
[§]Magnetic Resonance Center CERM, University of Florence, Via Luigi Sacconi 6, 50019, Sesto Fiorentino, Florence, Italy
[∥]Department of Gene Technology, Tallinn University of Technology, Akadeemia tee 15, 12618 Tallinn, Estonia

Supporting Information

ABSTRACT: The generation of [4Fe-4S] clusters in mitochondria critically depends, in both yeast and human cells, on two A-type ISC proteins (in mammals named ISCA1 and ISCA2), which perform a nonredundant functional role forming in vivo a heterocomplex. The molecular function of ISCA1 and ISCA2 proteins, i.e., how these proteins help in generating [4Fe-4S] clusters, is still unknown. In this work we have structurally characterized the Fe/S cluster binding properties of human ISCA2 and investigated in vitro whether and how a [4Fe-4S] cluster is assembled when human ISCA1 and ISCA2 interact with the physiological $[2Fe\text{-}2S]^{2+}$ cluster-donor human GRX5. We found that (i) ISCA2 binds either [2Fe-2S] or [4Fe-4S] cluster in a dimeric state, and (ii) two molecules of $[2Fe\text{-}2S]^{2+}$ GRX5 donate their cluster to a heterodimeric ISCA1/ISCA2 complex. This complex acts as an "assembler" of [4Fe-4S] clusters; i.e., the two GRX5-donated $[2Fe\text{-}2S]^{2+}$ clusters generate a $[4Fe\text{-}4S]^{2+}$ cluster. The formation of the same $[4Fe\text{-}4S]^{2+}$ cluster-bound heterodimeric species is also observed by having first one $[2Fe\text{-}2S]^{2+}$ cluster transferred from GRX5 to each individual ISCA1 and ISCA2 proteins to form $[2Fe\text{-}2S]^{2+}$ ISCA2 and $[2Fe\text{-}2S]^{2+}$ ISCA1, and then mixing them together. These findings imply that such heterodimeric complex is the functional unit in mitochondria receiving [2Fe-2S] clusters from hGRX5 and assembling [4Fe-4S] clusters before their transfer to the final target apo proteins.

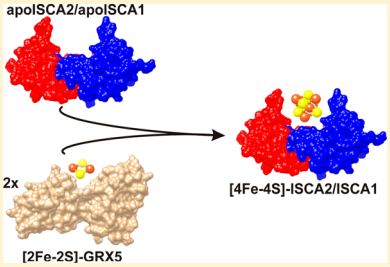

INTRODUCTION

In eukaryotes, mitochondria are central for iron–sulfur (Fe/S) protein biogenesis.[1] They harbor an iron–sulfur cluster (ISC) assembly machinery that is essential for the maturation of all [2Fe-2S] and [4Fe-4S] proteins, either located in the mitochondria, cytosol, or nucleus.[1,2] Two major steps are operative in the ISC assembly machinery. At first, seven proteins, termed core ISC assembly components, assemble de novo a [2Fe-2S] cluster and transfer it to monothiol glutaredoxin 5 (GRX5), which acts as Fe/S cluster transfer protein inserting the [2Fe-2S] cluster into mitochondrial [2Fe-2S]-requiring proteins.[3−5] The second step of the ISC assembly machinery is responsible for the generation of [4Fe-4S] clusters and their insertion into mitochondrial [4Fe-4S]-requiring proteins. At variance with the core ISC assembly components, the proteins involved in this second step are not required for the formation of mitochondrial [2Fe-2S] and cytosolic [4Fe-4S] clusters.[6−8] The generation of [4Fe-4S] clusters in mitochondria critically depends, in both yeast and human cells, on two A-type ISC proteins (in mammals named iron-sulfur cluster assembly 1 (ISCA1) and iron-sulfur cluster assembly 2 (ISCA2)) and on IBA57 protein (iron-sulfur cluster assembly factor for biotin synthase- and aconitase-like mitochondrial proteins, with a mass of 57 kDa).[6−11] These three proteins functionally interact with each other, but IBA57 is not required for iron/iron–sulfur cluster binding to the ISCA proteins.[9] Deletion of each of their genes elicits highly similar phenotypes indicating that they cooperate in the same process.[6,8,9,12] Studies in yeast[6] also showed that (i) Isa1 and Isa2 (the homologous proteins to ISCA1 and ISCA2) perform a nonredundant role because they cannot functionally replace each other; (ii) they function in a heterocomplex; (iii) the close bacterial relatives, IscA, SufA (sulfur utilization factor A) and ErpA (essential respiratory protein A), can complement Isa1, but not Isa2.

The A-type ISC proteins have three highly conserved cysteine residues in a C-X_n-C-G-C sequence motif (n is usually 63–65, but is increased by a 21-residue insert in some eukaryotic proteins such as *Saccharomyces cerevisiae* Isa2), which was shown to be implicated, directly or indirectly, in iron and Fe/S cluster binding.[13−18] On the basis of in vivo yeast mutagenesis studies,[19,20] all the three conserved cysteines are essential for function. Structures of some bacterial IscA or SufA proteins have been determined in the apo form showing all the same fold.[21−24] These structures are, however, of limited utility

Received: July 31, 2014
Published: October 27, 2014

dx.doi.org/10.1021/ja507822j | J. Am. Chem. Soc. 2014, 136, 16240–16250

for describing the Fe or Fe/S cluster binding mode, as the C-terminal conserved CGC motif is generally not observed, presumably because of conformational flexibility. Moreover, two structures of IscA from *Escherichia coli*[21,24] were both tetrameric rather than dimeric as preferentially they are in solution.[25] Only *E. coli* SufA crystallized in a dimeric form with the CGC motif observable in one molecule of the dimer.[22] Computer modeling of the C-terminal region performed on this structure suggested that the four cysteine residues of the CGC motif of the two subunits are located at the dimer interface, in close proximity one another and hence available for Fe or Fe/S cluster binding.[22] More recently, the crystal structure of a [2Fe-2S] cluster-bound form of *Thermosynechococcus elongatus* IscA showed, however, a different coordination mode. Indeed, the structure is formed an asymmetric, domain-swapped tetramer formed by two α and two β subunits,[16] in which the [2Fe-2S] cluster is coordinated by two conformationally distinct α and β subunits, with asymmetric cluster coordination by Cys 37, Cys 101, Cys 103 from α and Cys 103 from β. The domain swapping has been, however, attributed to a crystallization artifact.[14]

All the structural and functional data from the literature were not able to provide a conclusive picture of the Fe/S cluster binding mode in ISCA proteins nor to describe the molecular function of ISCA1 and ISCA2 proteins, i.e., how these proteins help in generating [4Fe-4S] clusters. We have recently shown that human GRX5, which is able to receive a [2Fe-2S] cluster from the core ISC assembly components,[26] can transfer it to both human ISCA1 and ISCA2 through a cluster-mediated protein−protein interaction event.[27] This study[27] and the fact that yeast Isa1 and Isa2 form a complex in vivo[6] suggest that these two proteins might cooperate in molecular terms for the conversion of the two hGRX5-received [2Fe-2S] clusters into a [4Fe-4S] moiety. In this work we have structurally characterized the Fe/S cluster binding properties of human ISCA2 and investigated in vitro whether and how a [4Fe-4S] cluster is assembled when the three human proteins GRX5, ISCA1 and ISCA2 (hGRX5, hISCA1, hISCA2 hereafter) are made to interact together. We found that hISCA1 and hISCA2 form a heterodimeric complex, which acts as an "assembler" of [4Fe-4S] clusters; i.e., the two hGRX5-donated $[2Fe\text{-}2S]^{2+}$ clusters generate a $[4Fe\text{-}4S]^{2+}$ cluster. These findings suggest that the heterodimeric complex is the functional unit in mitochondria assembling [4Fe-4S] clusters before their transfer to the target apo proteins.

EXPERIMENTAL SECTION

Protein Production. Human GRX5, ISCA1 and ISCA2 proteins were expressed and purified as previously described.[27] $[2Fe\text{-}2S]^{2+}$ hGRX5 was obtained as previously reported.[27] The oxidized $[2Fe\text{-}2S]^{2+}$ cluster-bound form of hISCA2 ("as purified" hISCA2) was obtained from an anaerobic purification procedure. Apo hISCA2 was obtained by treatment of the aerobically purified protein with 100 mM EDTA and 20 mM ferricyanide. Apo hISCA1 was directly obtained from an anaerobic purification procedure. hISCA2, hISCA1 and the hISCA2/hISCA1 complex were chemically reconstituted in 50 mM Tris-HCl, 100 mM NaCl, 2 mM DTT buffer at pH 8 under anaerobic conditions incubating the "as purified" hISCA2, apo hISCA1 and apo hISCA1/hISCA2 complex, respectively, with two- to 5-fold $(NH_4)_2Fe(SO_4)_2$ and Na_2S for 2−16 h at room temperature. To follow cluster transfer between hGRX5 and the heterodimeric complex in the NMR experiments, the $[2Fe\text{-}2S]^{2+}$ cluster-bound form of hISCA1 was also obtained by adding 1 equiv of $[2Fe\text{-}2S]^{2+}$ hGRX5 to apo hISCA1 as previously described.[27]

Analytical Gel Filtration and UV−Visible. The aggregation state of the apo forms of hISCA2 and of the heterodimeric hISCA1/hISCA2 complex was analyzed using analytical gel filtration. Purified samples were loaded on a SuperdexTM 75 HR 10/30 analytical column (Amersham Bioscience). Protein concentration was 100 μM. Degassed 50 mM phosphate buffer (pH 7.0), and 5 mM DTT was used as an eluent.

UV−visible spectra of "as purified" and chemically reconstituted hISCA2, as well as of all hGRX5/hISCA1/hISCA2 protein mixtures was performed in degassed 50 mM phosphate buffer at pH 7, 5 mM DTT, 5 mM GSH on a Cary 50 Eclipse spectrophotometer. The absorbance ratio of A_{340}/A_{414} of chemically reconstituted hISCA2 is less than 1.3 as reported in four-cysteine-ligated ferredoxins.

ESI-MS. For ESI-MS analysis 20 μM samples of hISCA2 in 20 mM ammonium acetate, pH 7.5 were injected into the electrospray ion source of a QSTAR Elite ESI-Q-TOF MS instrument (Applied Biosystems, Foster City, USA) by a syringe pump at 8 μL/min and ESI-MS spectra were recorded during 5 min in the m/z region from 500 to 3000 Da with the following instrument parameters: ion spray voltage 5500 V; source gas 55L/min; curtain gas 20 L/min; declustering potential 60 V; focusing potential 320 V; detector voltage 2550 V. In cluster stability experiments an increasing concentration of ferricyanide or DTT were added to 20 μM samples of chemically reconstituted hISCA2. Samples were then incubated for 2 min, and finally analyzed by ESI-MS.

EPR Spectroscopy. EPR spectra of chemically reconstituted hISCA2 samples were obtained using a Bruker Elexsys E500 spectrometer working at a microwave frequency of ca. 9.45 GHz and equipped with a SHQ cavity and a continuous flow He cryostat (ESR900, Oxford instruments) for temperature control. Acquisition parameters were as following: sample temperature, 45 K; microwave frequency, 9.640928 GHz; microwave power, 5 mW; modulation frequency, 100 kHz; modulation amplitude, 2.0 G; acquisition time constant, 163.84 ms; number of points 1024; number of scans 8; field range 2300−4300 G.

NMR Spectroscopy. All NMR experiments used for resonance assignment for either apo or chemically reconstituted hISCA2 were recorded on Bruker AVANCE 500, BRUKER AVANCE III 950, and Bruker AVANCE 700 spectrometers on ^{13}C,^{15}N-labeled samples in 50 mM phosphate buffer, pH 7.0, containing 10% (v/v) D_2O and 5 mM DTT. All NMR spectra were collected at 298 K, processed using the standard BRUKER software (Topspin 2.1) and analyzed through the CARA program.[28] The ^1H, ^{13}C and ^{15}N resonance assignment for both protein states were performed acquiring HNCO, HNCOCA, HNCA, CBCACONH, CBCANH for backbone assignment, and 2D TOCSY and hCCH-TOCSY, HBHA(CBCACO)NH experiments for side chain assignment (chemical shifts file of apo hISCA2 provided as Supporting Information). For the apo form, 101 of the expected 108 $[^1H-^{15}N]$ backbone resonances were assigned. The missing NH resonances are located in loop 3 (Cys 79) and in the C-terminal region of the protein (residues 126−130 and 132). ϕ and ψ backbone dihedral angle constraints were derived from the Chemical Shifts Index (CSI) analysis with TALOS+ program.[29] ^{15}N heteronuclear relaxation experiments on ^{15}N-labeled apo and chemically reconstituted hISCA2, on a 1:1 protein mixture of ^{15}N-labeled apohISCA2/unlabeled apo hISCA1, on a 1:2 mixture of unlabeled apo hISCA2/hISCA1 complex and ^{15}N-labeled $[2Fe\text{-}2S]^{2+}$ hGRX5, on a 1:1:1 mixture of ^{15}N-labeled apo hISCA2/unlabeled $[2Fe\text{-}2S]^{2+}$ GRX5/unlabeled $[2Fe\text{-}2S]^{2+}$ hISCA1 were collected to measure ^{15}N backbone longitudinal (R_1) and transverse (R_2) relaxation rates and heteronuclear $^{15}N\{^1H\}$ NOEs.

To follow the formation of the heterodimeric complex formation, ^{15}N-labeled apo hISCA2 was titrated with increasing amounts of the unlabeled apo hISCA1 and ^{15}N-labeled apo hISCA1 with increasing amounts of unlabeled apo hISCA2. Chemical shift changes were followed in the $^1H-^{15}N$ HSQC spectra and the significant differences in chemical shifts between free and bound hISCA2 were mapped on the surface of the structural model of hISCA2.

The cluster transfer between $[2Fe\text{-}2S]^{2+}$ hGRX5 and the heterodimeric complex was followed by $^1H-^{15}N$ HSQC experiments titrating (i) the heterodimeric, unlabeled apo hISCA1/hISCA2

dx.doi.org/10.1021/ja507822j | J. Am. Chem. Soc. 2014, 136, 16240−16250

complex (1 equiv) with increasing amounts of ^{15}N-labeled [2Fe-2S]$^{2+}$ hGRX5 (up to 2.5 equiv), (ii) the ^{15}N-labeled apo hISCA2/unlabeled apo hISCA1 complex (1 equiv) with increasing amounts of unlabeled [2Fe-2S]$^{2+}$ hGRX5 (up to 2.5 equiv) and (iii) premixed ^{15}N-labeled apo hISCA2 (1 equiv)/unlabeled [2Fe-2S]$^{2+}$ hGRX5 (1 equiv) with [2Fe-2S]$^{2+}$ hISCA1 (1 equiv).

Paramagnetic ^{1}H NMR experiments were performed on a Bruker AVANCE600 spectrometer, equipped with a ^{1}H selective probe.[30,31] Experiments were performed using 85 and 230 ms as acquisition and recycle delay, respectively. Water presaturation was applied during the recycle delay with a selective pulse. Spectral window was 192 kHz. From 100 000 to 500 000 scans were acquired. Experimental time was varying from 9 to 48 h.

Fe/S Cluster Quantification. The level of cluster transferred from [2Fe-2S]$^{2+}$ hGRX5 to the apo hISCA1/hISCA2 complex was quantified performing the following procedure: (i) a 1:1 heterodimeric apo hISCA1/hISCA2 complex was prepared monitoring its complete formation through spectral changes observed in the ^{1}H−^{15}N HSQC maps of ^{15}N-labeled apo hISCA2 titrated with unlabeled hISCA1; (ii) this sample was split in two halves; (iii) one-half was then titrated with ^{15}N-labeled [2Fe-2S]$^{2+}$ hGRX5 up to ∼2 equiv, observing, by both ^{1}H−^{15}N HSQC NMR and UV−vis experiments, the formation of apo hGRX5 and holo hISCA1/hISCA2 complex (only 5−10% of [2Fe-2S]$^{2+}$ hGRX5, as estimated from the NMR data, remained in the final mixture); (iv) the other half of the apo hISCA1/hISCA2 complex was chemically reconstituted and the ^{1}H−^{15}N HSQC NMR and UV−vis spectra acquired; (v) on both (iii) and (iv) mixtures and on the ^{15}N-labeled [2Fe-2S] hGRX5 sample used to titrate the apo hISCA1/hISCA2 complex, the iron and inorganic sulfur content and the protein concentration were estimated following standard chemical assays[32,33] and reported in Table 1. Before the acquisition of spectroscopic and quantification data, (iii) and (iv) samples were passed through a PD10 desalting column in anaerobic conditions to remove interference of other components in the mixture, such as the species that could form upon interaction of iron ions with free sulfide, and the thiols of DTT and GSH.

Table 1. Iron and Acid-Labile Sulfide Analyses of hISCA2, hGRX5 and hISCA1/hISCA2 Complexes

sample	Fe[a]	S[a]
[4Fe-4S] ^{15}N-hISCA2/hISCA1 apo ^{15}N-hGRX5 mixture[b]	3.9 ± 0.1	3.8 ± 0.1
chemically reconstituted hISCA1/^{15}N-hISCA2 complex	3.7 ± 0.1	3.8 ± 0.1
chemically reconstituted ^{15}N-hISCA2	4.1 ± 0.1	3.9 ± 0.1
[2Fe-2S] ^{15}N-hGRX5	2.1 ± 0.1	2.0 ± 0.1

[a]Fe and acid-labile S measurements are reported as mol Fe or S per mol of homodimer or heterodimer. Fe and S measurements are the averages of two independent samples. [b]Protein concentration of hISCA1/hISCA2 complex was estimated subtracting the total amount of hGRX5 added in the mixture. Fe and S contribution derived from residual [2Fe-2S] hGRX5, estimated to 5−10% from ^{1}H−^{15}N HSQC NMR data, was subtracted from the total Fe and S content.

Structural Modeling and Analysis. To generate the structure model of monomeric apo hISCA2, assigned backbone (^{1}HN, ^{15}N, ^{13}Cα, ^{13}Cβ, ^{13}CO, and ^{1}Hα) chemical shifts were used as input in CS-ROSETTA program.[34] The structures of monomeric apo hISCA2 generated by CS-ROSETTA and MODELER[35] were used as input for docking calculations. The docking simulations of dimeric apo hISCA2 were obtained using the HADDOCK web server.[36] The residues taken into account to define the hISCA2 dimerization interface were Tyr 84, Phe 86, Ser 87, Glu 126, Leu 127, Ile 128, Arg 129, Ser 130, Ser 131, Phe 132, selected on the basis of conformational exchange processes detected by their line broadening effects on the NMR spectra. As constraints in the calculation of the dimer a C2 symmetry axis was also used, consistently with NMR spectra of apo hISCA2, which indicate that dimer subunits interact on average in a symmetric way to produce degenerate resonances for both molecules.

RESULTS

Structural and Fe/S Binding Properties of Human ISCA2. A construct of human ISCA2 lacking the N-terminal mitochondrial targeting sequence responsible of its import in the mitochondrial matrix (hISCA2 hereafter, residues 44−154) was recombinantly expressed in *E. coli* cells as previously reported.[27] After its purification in anaerobic conditions, analytical gel filtration showed that the protein at 100 μM (about 10-fold lower than protein concentration used in the NMR experiments, 1 mM) elutes as a dimer, which is in a mixture of apo and [2Fe-2S] cluster bound species ("as purified" hISCA2, hereafter), as reported later in this article. ^{1}H−^{15}N HSQC spectrum of apo hISCA2, obtained as described in Experimental Section, shows well-dispersed NH signals indicative of an essentially folded protein (Figure 1A). On the basis of the CSI and backbone NOEs analysis of apo hISCA2, it results that the vast majority of residues in the protein segment 50−140 form secondary structural elements (50−52 (strand β1), 54−63 (helix α1), 69−75 (strand β2), 83−88 (strand β3), 98−101 (strand β4), 104−108 (strand β5), 110−115 (helix α2), 120−124 (strand β6) and 131−135 (strand β7)). A three-dimensional structural model of the monomeric subunit of apo hISCA2, calculated by CS-ROSETTA[34] using ^{1}HN, ^{15}N, ^{13}Cα, ^{13}Cβ, ^{13}CO, and ^{1}Hα chemical shifts, showed that residues 50−140 are folded into a single domain containing two α-helices and seven β-strands, adopting the same protein topology and the same protein fold of bacterial IscA/SufA proteins.[21,22,24] Backbone ^{15}N relaxation data showed that the overall reorientational correlation time of apo hISCA2 is 13.6 ± 1.2 ns, consistent with a molecule of about 24 kDa, thus indicating the dimeric state of apo hISCA2 (theoretical MW from hISCA2 sequence is 12.5 kDa). Backbone ^{15}N relaxation data (Figure 1B) also showed that the domain formed by residues 50−140 is rigid, with the exception of two loop regions (residues 65−68 and 76−82), which showed low ^{15}N{^{1}H} NOEs indicative of rapid internal motions on the picosecond to nanosecond time scale. The second loop contains Cys 79, which is the first of the three cysteines in the conserved C-X$_n$-C-G-C motif and which was suggested to be implicated in Fe/S cluster formation by coordinating an iron ion of the cluster or by stabilizing the Fe/S cluster binding.[22,37,38] The C-terminal tail (residues 141−154) of hISCA2, which contains the other two of the three conserved cysteines, is flexible (Figure 1B) and unstructured as shown by the CSI analysis. Therefore, the regions containing the three conserved Cys residues (residues 76−82 and the C-terminal tail) are all flexible and thus able of structural rearrangements to accommodate the cluster. Apo hISCA2 has the same structural organization of *E. coli* IscA protein in its apo state, i.e., a folded and rigid domain followed by an unstructured C-terminal tail, but presents a different quaternary structure (i.e., dimer vs tetramer).[21,24] The I-TASSER server, a platform for protein structure and function predictions,[39] identified the dimeric *E. coli* SufA crystal structure as the most confident PDB hit for modeling hISCA2 structure with 54% of sequence similarity. Moreover, at variance of *E. coli* IscA which in solution is present in a mixture of dimers and tetramers[25] and crystallized as a tetramer, both hISCA2 and SufA[22] are dimeric. These data therefore support that apo hISCA2 dimerizes in a way similar to apo SufA, differing from *E. coli* IscA protein which forms dimers

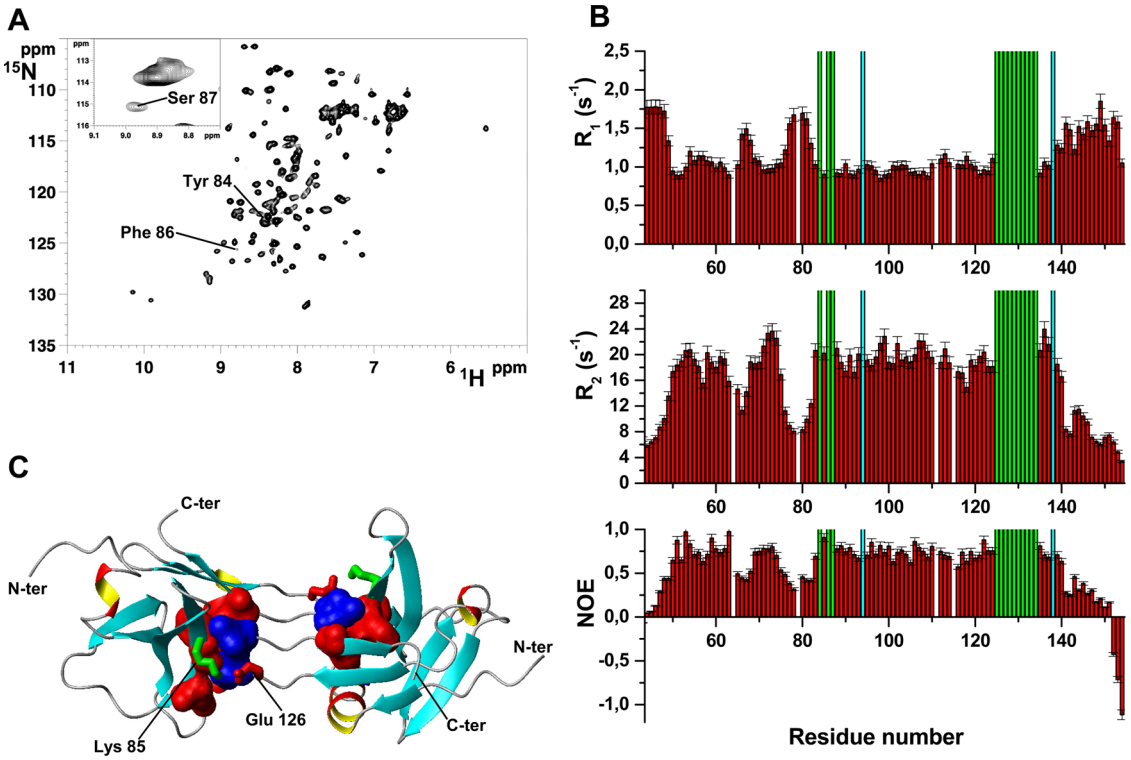

Figure 1. Structure and dynamic characterization of apo hISCA2. (A) $^{1}H-^{15}N$ HSQC spectrum of apo hISCA2. Some of broad amide protons at the dimeric interface are indicated in the $^{1}H-^{15}N$ HSQC spectrum and in the inset. (B) Experimental ^{15}N R_1, R_2 and heteronuclear $^{15}N\{^{1}H\}$ NOEs versus residue number of apo hISCA2 at 600 MHz in 50 mM phosphate buffer pH 7.0, 5 mM DTT. The cyano bars represent proline residues. The green bars represent residues whose NHs are not detected or too broad to be analyzed. Residues 64, 111, and 115 are excluded from the analysis as overlapped with side chain Asn/Gln amides. (C) Ribbon representation of the docking model of dimeric apo hISCA2 where the hydrophobic patches formed by Phe 86, Leu 88 and Phe 132 (in red) and by Leu 127 and Ile 128 (in blue) are shown. α-Helices are depicted in red/yellow and β-strands are in cyano. The intersubunit salt bridge formed between the Lys 85 (in green) and Glu 126 (in red) is also shown.

of dimers.[21,24] In the structure of apo SufA,[22] strands β6 and β7 and the loop between them are involved in the subunit−subunit contacts with strand β3, such interactions stabilizing the SufA dimeric state. In apo hISCA2, the NHs of residues corresponding to those located at the dimeric interface of SufA (residues 84, 86, 87 and 126−132 in apo hISCA2) are not detected or very broad in the $^{1}H-^{15}N$ HSQC map (Figure 1A and 1B). These effects are a consequence of conformational exchange processes, as confirmed by the temperature dependence of $^{1}H-^{15}N$ HSQC spectra which showed NH signals of the detected residues at the dimeric interface narrowing when lowering the temperature from 298 to 283 K. Such backbone conformational flexibility might be caused by dynamic processes on the two subunits at the dimer interface. To examine whether this flexible region is actually involved in the subunit−subunit contacts, residues 84, 86, 87 and 126−132 were used to generate a docking model of dimeric apo hISCA2 (coordinate file of the 3D structural model provided as Supporting Information) calculated through HADDOCK program.[40] It results that only one cluster of structures was obtained containing 200 structures with a backbone root-mean-square deviation to the mean structure of 0.8 ± 0.5 Å and a buried surface area of 1241 ± 71 Å^2 indicative of a good surface complementarity (Table S1). These results unambiguously show that dimerization of hISCA2 occurs through the same intersubunit contact region as observed in SufA. The main contacts at the subunit−subunit interface are provided by a hydrophobic patch involving residues Phe 86, Leu 88 and Phe 132 from one subunit and residues Leu 127 and Ile 128 from the other (Figure 1C). An intersubunit salt bridge between Lys 85 and Glu 126 (Figure 1C) also stabilizes the dimer−dimer interface.

The Fe/S cluster binding properties of hISCA2 were investigated by ESI-MS, EPR and paramagnetic ^{1}H NMR spectroscopies. ESI-MS data (Figure 2A) showed that "as purified" hISCA2 is mainly monomeric (1:1 mixture of apo hISCA2 and Fe_1hISCA2 forms), at variance of what observed by gel filtration and NMR ^{15}N relaxation data. This can be a consequence of the backbone flexibility observed at the dimeric interface that destabilizes the dimer in the ESI-MS ionization conditions. However, ESI-MS data showed that "as purified" hISCA2 also contains a [2Fe-2S] cluster-bound dimeric species, consistent with gel filtration and UV−vis spectrum (see later). The 1D ^{1}H paramagnetic NMR spectrum (trace **a** in Figure 2B) and the temperature dependence of its paramagnetic signals (Figure S1) showed a behavior typical of a $[2Fe\text{-}2S]^{2+}$ cluster-containing species, thus confirming the presence, in the "as purified" hISCA2 protein, of a $[2Fe\text{-}2S]^{2+}$ cluster bound species. Chemical reconstitution leads to the formation of a [4Fe-4S]-bound, dimeric species ([4Fe-4S] hISCA2 hereafter, Table 1 and traces **b** in Figure 2A and 2B). A dimeric [2Fe-2S] cluster bound species is also detected at a low level (~10%) by ESI-MS data (Figure 2A) and by 1D ^{1}H NMR spectrum (trace **b** in Figure 2B). ESI-MS data also shows that no dimeric, Fe-only bound species are detected (Figure 2A) at variance of what observed for bacterial IscA proteins.[14,41] Only the binding of a [2Fe-2S] or a [4Fe-4S] cluster is therefore sufficient to stabilize the dimeric state of hISCA2 in the ESI-MS experiment,

dx.doi.org/10.1021/ja507822j | J. Am. Chem. Soc. 2014, 136, 16240−16250

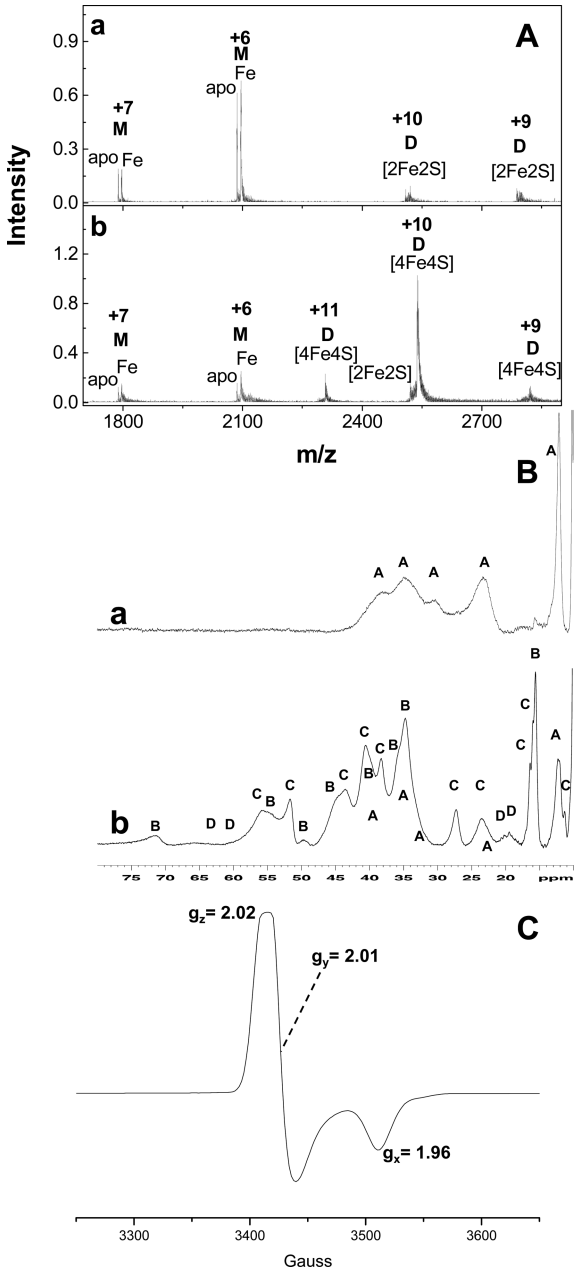

Figure 2. Fe/S binding properties of hISCA2. (A) ESI-MS spectra of "as purified" hISCA2 (a) and of chemically reconstituted hISCA2 (b). Conditions: 20 μM protein concentration, 20 mM ammonium acetate, pH 7.5, T = 298 K. +7 and +6 charge states are presented for apo and Fe hISCA2 monomer (M); +11, +10 and +9 charge states are presented for [2Fe-2S] and [4Fe-4S] hISCA2 dimers (D). Metal or Fe/S cluster contents are indicated on the top of the peaks. (B) Paramagnetic 1D ^{1}H NMR spectra of "as purified" $[2Fe\text{-}2S]^{2+}$ hISCA2 (a) and of chemically reconstituted hISCA2 (b) in 50 mM phosphate buffer pH 7.0 at 600 MHz and 283 K. Signals labeled A arise from Hβ and Hα from cysteine ligands coordinated to a $[2Fe\text{-}2S]^{2+}$ cluster. Signals labeled B, C and D arise from Hβ and Hα from cysteine ligands coordinated to a $[4Fe\text{-}4S]^{+}$ cluster in different species that have been identified according to relative intensities of signals B–D observed in different reconstituted protein samples. (C) EPR spectra at 45 K (50 mM phosphate, 5 mM DTT buffer at pH 7, 10% glycerol) of [4Fe-4S] hISCA2 obtained by chemical reconstitution. The g-values are indicated.

suggesting that the Fe/S cluster bridges two hISCA2 molecules through their cysteine ligands. These results again indicate a quaternary structural organization of dimeric hISCA2 similar to that of *E. coli* SufA[22] and different from that of *E. coli* IscA.[21,24] Indeed, in the dimeric unit of *E. coli* IscA structure, two of the three invariant cysteine ligands of the Fe/S cluster (Cys 142 and Cys 144) in the two subunits α1 and α2 are far from each other, making the cluster binding possible only upon formation of the tetrameric form.[21,24] ESI-MS data of either [2Fe-2S] or [4Fe-4S] hISCA2 show that the protein is in dimeric form only and does not form tetramers, thus ruling out the subunit $\alpha1\alpha2$ arrangement found in the tetrameric structure of *E. coli* IscA.

EPR (Figure 2C) and 1D paramagnetic NMR spectra (Figure 2B) of [4Fe-4S] hISCA2 are consistent with the presence of at least three species with signals typical of a $[4Fe\text{-}4S]^{+}$ bound-cluster and of a minor, EPR-silent, species with signals from a $[2Fe\text{-}2S]^{2+}$ bound-cluster. The temperature dependence of the paramagnetic NMR signals (Figure S1) reveals that the electronic distribution within the $[4Fe\text{-}4S]^{+}$ cluster is different from that observed in bacterial ferredoxins,[42,43] where the protein scaffold around the cluster has no symmetry, thus determining different environments and consequently different electronic properties for each iron ion. In the present protein, hISCA2, the cluster is at the interface of two identical monomers, therefore the scaffold around the cluster is highly symmetric, thus making the four iron ion essentially equivalent. This, on its turn, produces a large electron delocalization,[44] which decreases the effective J values among the iron ions, determining downfield shifts and anti-Curie temperature dependence for signals from all Cys βCH_2.[45−47]

Changes in the redox conditions affect the nature of the cluster bound to hISCA2. Indeed, upon addition of ferricyanide up to 1.5 equiv, ESI-MS and 1D ^{1}H paramagnetic NMR data (Figure S2) showed that the level of the dimeric $[4Fe\text{-}4S]^{+}$ hISCA2 decreases while that of the dimeric $[2Fe\text{-}2S]^{2+}$ hISCA2 species increases, suggesting the occurrence of a [4Fe-4S] → [2Fe-2S] cluster conversion process in which oxidized $[4Fe\text{-}4S]^{2+}$ cluster is rapidly converted into a $[2Fe\text{-}2S]^{1+}$ form which is finally oxidized to the $[2Fe\text{-}2S]^{2+}$ form. A similar behavior was observed for the bacterial ^{Nif}IscA, which experienced O_2-induced $[4Fe\text{-}4S]^{2+}$ oxidative cleavage to produce ^{Nif}IscA-bound $[2Fe\text{-}2S]^{2+}$ clusters.[15] When DTT is added to dimeric [4Fe-4S] hISCA2, ESI-MS data (Figure S2) showed that the amount of dimeric [4Fe-4S] hISCA2 decreases, and correspondingly the amount of monomeric apo protein increases. At variance with oxidation, no formation of a dimeric [2Fe-2S] hISCA2 species is detected upon reduction, but only low levels of monomeric [2Fe-2S] hISCA2 species are formed (Figure S2). This indicates that DTT in excess substitutes protein ligands, breaking hISCA2 dimeric state, and then extracts the cluster from the protein, i.e., [4Fe-4S] hISCA2 dimer → [2Fe-2S] hISCA2 monomer → apo monomer.

Backbone ^{15}N relaxation data (Figure 3A) show that the overall reorientational correlation time of [4Fe-4S] hISCA2 is 15.7 ± 2.0 ns, indicating that [4Fe-4S] cluster binding does not induce alteration in the quaternary structure of hISCA2, which remains indeed dimeric as it is in the apo form. The ^{1}H−^{15}N HSQC map of [4Fe-4S] hISCA2 (Figure 3B) is largely superimposable to that of the apo form, indicating that cluster binding does not affect the structure. Significant chemical shift changes (Figure 3C) were, however, observed for residues 112−116 (helix α2), which are spatially close to the conserved Cys 79 and to the C-terminal tail, for residues 85−87, 125, 131 located at the dimeric interface, and for residues 136, 139, 140,

dx.doi.org/10.1021/ja507822j | J. Am. Chem. Soc. 2014, 136, 16240−16250

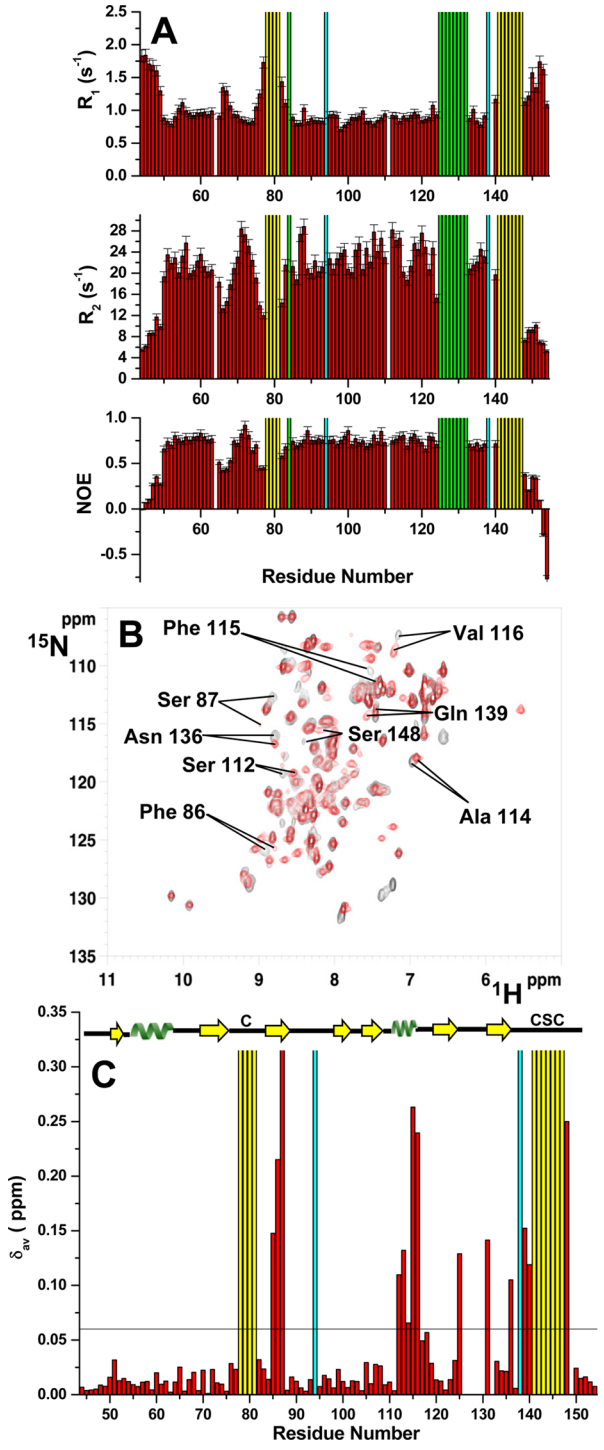

Figure 3. Structure and dynamic characterization of [4Fe-4S] hISCA2. (A) ^{15}N R_1, R_2 and ^{15}N{^{1}H} NOEs versus residue number of chemically reconstituted [4Fe-4S] hISCA2 collected at 600 MHz in 50 mM phosphate buffer pH 7.0, 5 mM DTT. The cyano bars represent proline residues. The green bars represent residues whose NHs are not detected or too broad to be analyzed. The yellow bars represent the NH signals broadened beyond detection as a consequence of the binding of the paramagnetic [4Fe-4S] cluster. Residues 64, 111, and 139 are excluded from the analysis as overlapped with side chain Asn/Gln amides. (B) Superposition of ^{1}H−^{15}N HSQC spectra of apo hISCA2 (red) and chemically reconstituted [4Fe-4S] hISCA2 (black). Some of the residues showing chemical shift changes upon cluster binding are indicated. (C) Weighted-average chemical shift differences δ_{av} (that is, $([(\delta_{HN})^2 + (\delta_N/5)^2]/2)^{1/2}$, where δ_{HN} and δ_N are chemical shift differences for ^{1}HN and ^{15}N, respectively) between apo hISCA2 and chemically reconstituted [4Fe-4S] hISCA2. The cyano bars represent proline residues. The yellow bars represent the NH signals broaden beyond detection as a consequence of the binding of the paramagnetic [4Fe-4S] cluster.

148, which are in the unstructured C-terminal region containing the conserved CXC motif (where X = Ser in hISCA2). Moreover, the NH signals of the residues 78−81 and 141−147 containing, respectively, Cys 79 and the CSC motif broaden beyond detection (Figure 3C). The line broadening effects observed for these two regions containing the three putative cysteine ligands and the chemical shifts on helix α2 are a consequence of the binding of the paramagnetic [4Fe-4S] cluster, which induces only local structural rearrangements at the dimeric interface.

hISCA2 Forms a Heterodimeric Complex with hISCA1. When ^{15}N-labeled apo hISCA2 is titrated with increasing amounts of unlabeled apo hISCA1 or ^{15}N-labeled apo hISCA1 with increasing amounts of unlabeled apo hISCA2, the ^{1}H and ^{15}N resonances in the ^{1}H−^{15}N HSQC spectra exhibit spectral changes as a function of the amounts of the unlabeled protein (Figure 4A). In particular, the signals of ^{15}N-labeled apo hISCA2 or apo hISCA1 species decrease in intensity while a new set of signals increases by increasing the amounts of the partner protein, indicating that the two proteins interact and exchanges slowly on the NMR time scale. An upper limit value of about 10 μM can be estimated, from the NMR data, for the K_d of the heterodimer formation, consistent with its physiologically relevance. Spectral changes are completed at the ∼1:1 protein ratio (Figure 4A), indicating that the two proteins form a 1:1 protein−protein complex. The ^{1}H and ^{15}N chemical shift differences between apo hISCA2 alone and in the 1:1 protein complex, once mapped on the structural model of dimeric apo hISCA2, showed that the major changes (1σ Δ_{avg}(HN) > 0.05 ppm) are localized in a well-defined region of the protein (involving residues 59−60, 67−68, 74, 84−88, 123−125 and 131), consistent with a specific recognition pattern (Figure 4B and 4C). This region matches with the subunit−subunit interface stabilizing the dimer in the structural model of hISCA2 (Figure 4C), thus indicating that apo hISCA1 and apo hISCA2 are interacting each other by forming a dimeric structure similar to that of homodimeric hISCA2. ^{15}N R_2 and ^{15}N R_1 experiments, performed on the 1:1 protein mixture, provided a molecular tumbling τ_m of 16.0 ± 2.7 ns, which is the same value found for dimeric hISCA2. At variance with the homodimer, R_2 values of several residues at the interface in the heterodimer can be determined, indicating a slower conformational exchange process. We can therefore conclude that the heterodimeric adduct is formed by substituting a subunit of homodimeric apo hISCA2 with apo hISCA1, which exists in a monomer−dimer equilibrium in solution,[27] thus indicating that heterodimer formation is thermodynamically favored with respect to that of the homodimer. In support to this conclusion, the comparison of the final ^{1}H−^{15}N HSQC experiments in the two titrations (Figure S3) pointed out that spectral variations are much more dramatic in hISCA1 than on hISCA2, because hISCA1 passes from a dimer/monomer equilibrium to a dimeric state, while hISCA2 remains in a dimeric state that involve the same subunit−subunit interface in both homo- and heterodimers.

dx.doi.org/10.1021/ja507822j | J. Am. Chem. Soc. 2014, 136, 16240−16250

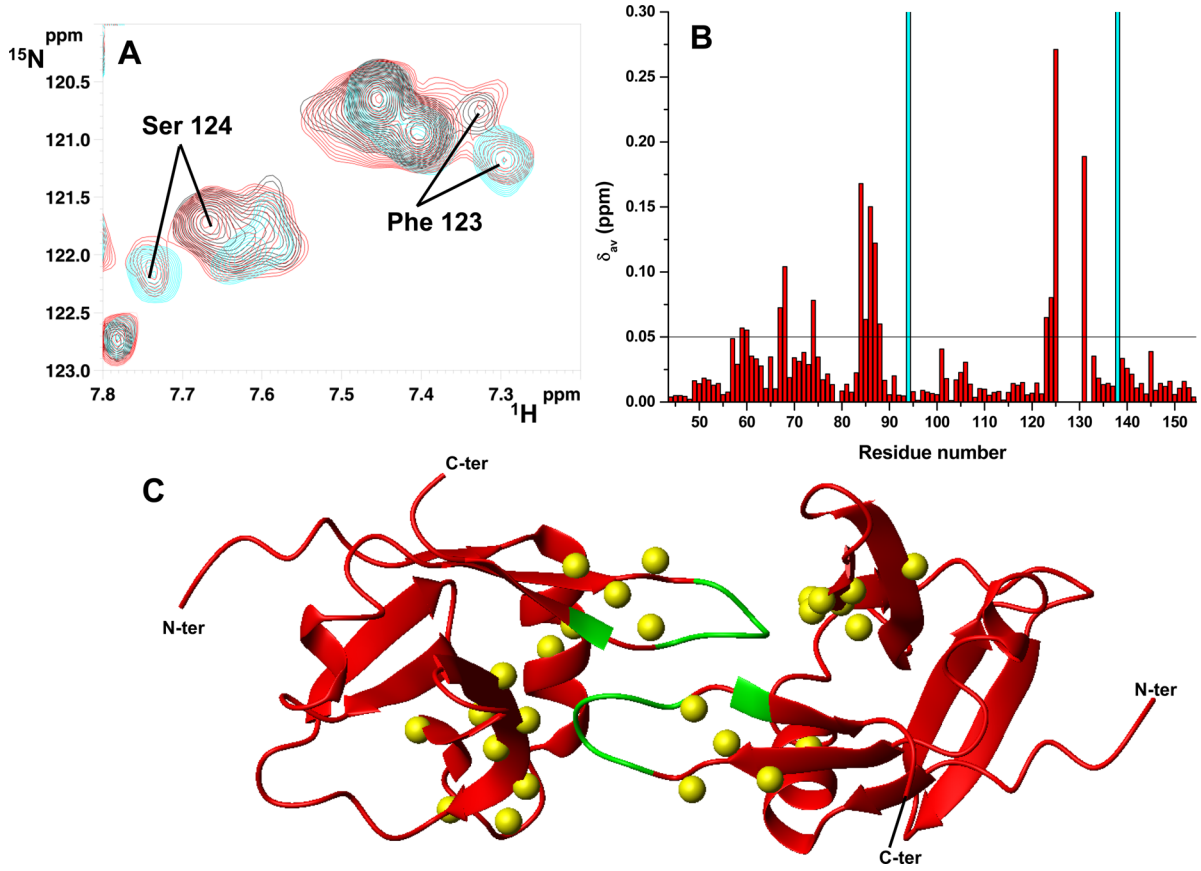

Figure 4. Heterodimeric complex formation between apo hISCA1 and apo hISCA2. (A) $^{1}H-^{15}N$ HSQC spectra of two residues (Phe 123 and Ser 124) representative for apo hISCA2 free and in complex with apo hISCA1 are shown in the absence (black) or in the presence of 0.5 equiv (red) and 1 equiv (cyano) of apo hISCA1. (B) Weighted-average chemical shift differences δ_{av} (that is, $([(\delta_{HN})^2 + (\delta_N/5)^2]/2)^{1/2}$, where δ_{HN} and δ_N are chemical shift differences for ^{1}HN and ^{15}N, respectively) between free apo hISCA2 and apo hISCA2 in a 1:1 complex with unlabeled apo hISCA1. The cyano bars represent proline residues. (C) Significant chemical shift changes ($1\sigma\ \Delta_{avg}$(HN) > 0.05 ppm) of backbone NHs occurring on ^{15}N-labeled apo hISCA2 upon addition of 1 equiv of unlabeled apo hISCA1 are mapped on the structural model of dimeric apo hISCA2 as yellow spheres. The protein stretches in green represent unassigned NHs in apo hISCA2.

$[2Fe\text{-}2S]^{2+}$ hGRX5 Transfers Its Cluster to the Heterodimeric hISCA1-hISCA2 Complex. ^{15}N-labeled $[2Fe\text{-}2S]^{2+}$ hGRX5 was titrated with increasing amounts of unlabeled heterodimeric apo hISCA1/hISCA2 complex. Once 2 equiv of $[2Fe\text{-}2S]^{2+}$ hGRX5 were added to 1 equiv of hISCA1/hISCA2 complex, the $^{1}H-^{15}N$ HSQC spectrum fully matched that of apo hGRX5 (Figure 5A), suggesting that hGRX5 transfers its $[2Fe\text{-}2S]^{2+}$ cluster to the heterodimeric hISCA2/hISCA1 complex. Since the NH signals of $[2Fe\text{-}2S]^{2+}$ hGRX5 were detected in the $^{1}H-^{15}N$ HSQC map only when a complex/protein ratio higher than 1:2 was reached, as reported in the plot of Figure 5A, two $[2Fe\text{-}2S]^{2+}$ clusters are transferred from hGRX5 to the heterodimeric complex. ^{15}N heteronuclear relaxation data of hGRX5 in the 1:2 mixture showed an increase of the molecular tumbling τ_m from 7.97 ± 0.63 ns (consistent with a monomeric protein state in solution[27]) to 10.72 ± 0.75 ns. This small increase might suggest the formation of a low-populated, transient protein−protein adduct in solution as already observed with the isolated proteins.[27] This is in agreement with a cluster transfer mechanism occurring via an associative process between hGRX5 and the heterodimeric complex. This mechanism fully support a functional role of hGRX5 as a $[2Fe\text{-}2S]^{2+}$ cluster transfer protein, which shuttles the $[2Fe\text{-}2S]^{2+}$ cluster from the core ISC assembly machinery to several target proteins.[26,27]

Similarly, when the heterodimeric apo hISCA1/hISCA2 complex, having hISCA2 ^{15}N-labeled, is titrated with increasing amounts of unlabeled $[2Fe\text{-}2S]^{2+}$ hGRX5 up to a ∼1:2 protein ratio, the $^{1}H-^{15}N$ HSQC spectrum, detecting hISCA2, shows the formation of a new species whose ^{1}H and ^{15}N chemical shifts compare well with those of a $[4Fe\text{-}4S]^{2+}$ cluster-bound form of the heterodimeric hISCA2/hISCA1 complex obtained by chemical reconstitution (Figure 5B). This new species is EPR silent and a UV−vis spectrum typical of $[4Fe\text{-}4S]^{2+}$ cluster proteins dominated by a broad shoulder centered at ∼420 nm (Figure 5B), consistent with the formation of a $[4Fe\text{-}4S]^{2+}$ cluster-bound complex assembled by a reductive coupling process of the two $[2Fe\text{-}2S]^{2+}$ hGRX5-donated clusters. $[4Fe\text{-}4S]^{2+}$ cluster formation on the heterodimeric complex was also observed by preforming $[2Fe\text{-}2S]^{2+}$ hISCA2 through the addition of 1 equiv of $[2Fe\text{-}2S]^{2+}$ hGRX5 to apo hISCA2, and then mixing it with 1 equiv of $[2Fe\text{-}2S]^{2+}$ hISCA1. $^{1}H-^{15}N$ HSQC and UV−vis spectra of both hGRX5/hISCA2/hISCA1 mixtures (i.e., obtained by mixing 2 equiv of $[2Fe\text{-}2S]^{2+}$ hGRX5 to the heterodimeric apo hISCA1/^{15}N-labeled hISCA2 complex (1 equiv) or by mixing 1 equiv of $[2Fe\text{-}2S]^{2+}$ hGRX5 with 1 equiv of ^{15}N-labeled apo hISCA2 and then adding 1 equiv of $[2Fe\text{-}2S]^{2+}$ hISCA1) are indeed fully superimposable. ^{15}N R_2 and ^{15}N R_1 data on hISCA2 in the two mixtures provided a molecular tumbling τ_m of 15.9 ± 2.2 ns for hISCA2, i.e., the

dx.doi.org/10.1021/ja507822j | J. Am. Chem. Soc. 2014, 136, 16240−16250

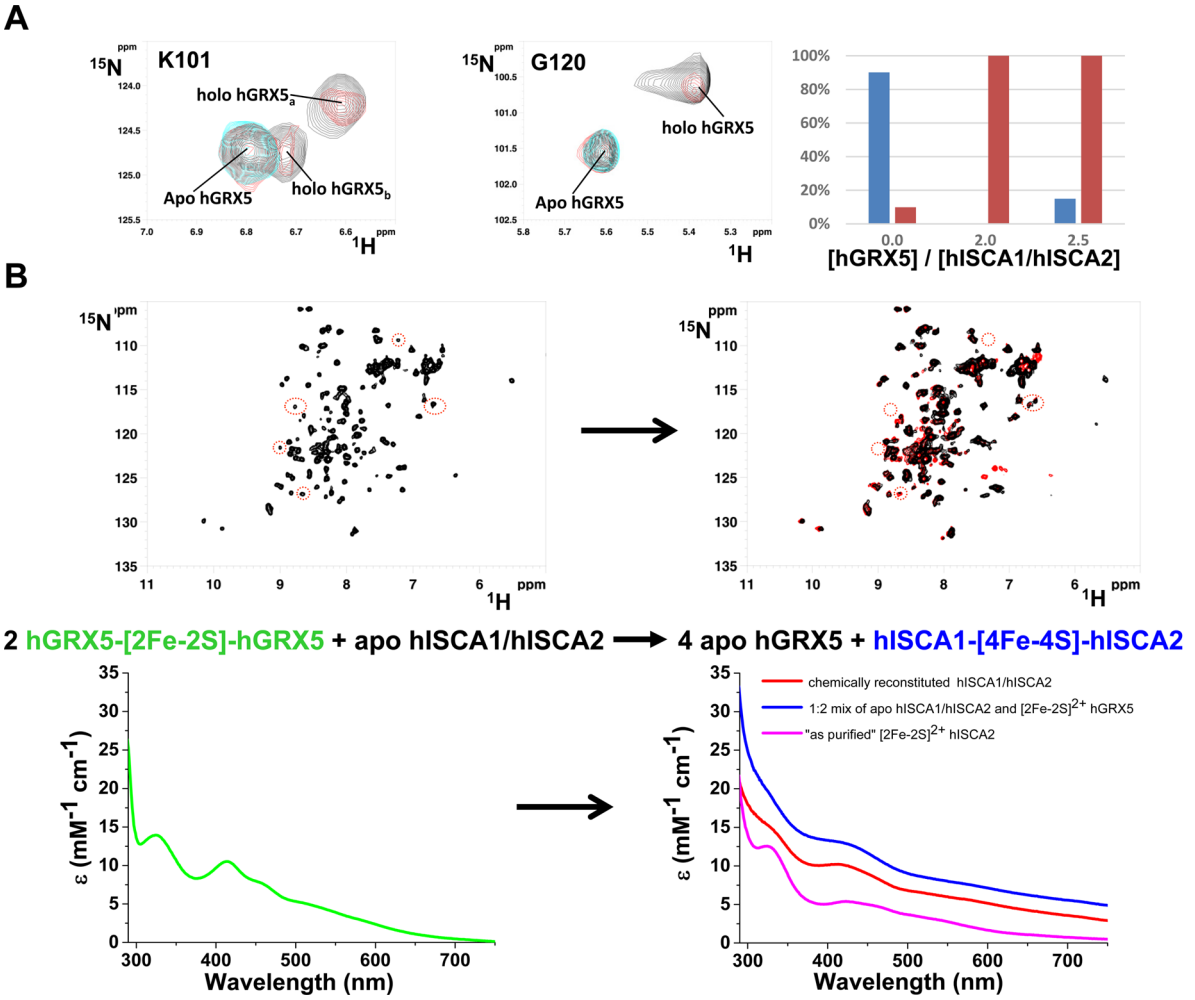

Figure 5. Formation of $[4Fe\text{-}4S]^{2+}$ cluster-bound hISCA1/hISCA2 complex upon addition of $[2Fe\text{-}2S]^{2+}$ hGRX5. (A) $^{1}H-^{15}N$ HSQC spectra of two residues (Lys 101 and Gly 120) selected to monitor cluster transfer between ^{15}N-labeled $[2Fe\text{-}2S]^{2+}$ hGRX5 and the unlabeled apo hISCA1/apo hISCA2 complex. Color code: $[2Fe\text{-}2S]^{2+}$ hGRX5 is in black; unlabeled apo hISCA1/apohISCA2 complex after the addition of $[2Fe\text{-}2S]^{2+}$ hGRX5 in a 1:2 (cyano) and 1:2.5 (red) protein ratios. The residues having two sets of signals in $[2Fe\text{-}2S]^{2+}$ hGRX5[27] are indicated with a and b labels. $[2Fe\text{-}2S]^{2+}$ hGRX5 contained a residual amount of apo form as already described.[27] Plot showing the amounts of apo hGRX5 (orange bar) and $[2Fe\text{-}2S]^{2+}$ hGRX5 (blue bar) as a function of hGRX5:hISCA1/hISCA2 complex molar ratio, as obtained integrating the signals of K101 and G120 in the $^{1}H-^{15}N$ HSQC spectra of hGRX5 along the titration experiment. (B) The formation of the $[4Fe\text{-}4S]^{2+}$ heterodimeric hISCA1/hISCA2 complex by the addition of unlabeled $[2Fe\text{-}2S]^{2+}$ hGRX5 to apo hISCA1/^{15}N-labeled apohISCA2 complex is monitored by $^{1}H-^{15}N$ HSQC (up) and UV–vis (bottom) spectra. On the left, $^{1}H-^{15}N$ HSQC and UV–vis spectra of the two reactants apo hISCA1/^{15}N-labeled hISCA2 complex and $[2Fe\text{-}2S]^{2+}$ hGRX5 are shown, respectively. On the right, $^{1}H-^{15}N$ HSQC and UV–vis spectra of the 1:2 mixture between apo hISCA1/^{15}N-labeled hISCA2 complex and $[2Fe\text{-}2S]^{2+}$ hGRX5 are shown, respectively. The $^{1}H-^{15}N$ HSQC spectrum of the latter mixture (black) is superimposed to a chemically reconstituted hISCA1/^{15}N-labeled hISCA2 complex (red), whose UV–vis spectrum shows the occurrence of a mixture of $[4Fe\text{-}4S]^{2+}$ and $[2Fe\text{-}2S]^{2+}$ species in a 90:10 ratio, as estimated from the Fe and S quantification (Table 1). Red circles indicate spectral differences in the $^{1}H-^{15}N$ HSQC spectra of hISCA1/^{15}N-labeled hISCA2 before and after $[4Fe\text{-}4S]^{2+}$ cluster assembly.

same value found in the complex between apo hISCA2 and apo hISCA1, thus indicating that, in both mixtures, hISCA2 is essentially associated with hISCA1 only to form a heterodimeric complex.

In order to evaluate the efficiency of the heterodimeric hISCA1/hISCA2 complex at assembling a [4Fe-4S] cluster, the amount of cluster transferred from $[2Fe\text{-}2S]^{2+}$ GRX5 to the apo complex has been quantified as described in the Experimental Section. As reported in Table 1, the Fe:S:hISCA1/hISCA2 ratio is 3.9:3.8:1.0, showing that the efficiency of the heterodimer at assembling a [4Fe-4S] cluster is at least 90% and confirming that 2 equiv of [2Fe-2S] clusters are transferred from hGRX5 to the heterodimeric hISCA1/hISCA2 complex.

DISCUSSION

Although Fe/S clusters formation can be achieved spontaneously in vitro with inorganic iron and sulfur sources,[48] the in vivo situation is more complex and requires the so-called Fe/S protein biogenesis systems. These systems were identified in both prokaryotes[49,50] and eukaryotes[51] and two main steps are observed in both kingdoms: a mechanism of Fe/S cluster assembly and a transfer process of the assembled Fe/S cluster to the apoproteins. Multiple factors have been proposed to mediate the delivery step and the so-called A-type proteins have received most of the attention so far. Several studies[50] on bacterial A-type proteins are now available showing a high functional complexity and redundancy of bacterial A-type proteins. Specifically, bacterial systems have several A-type

dx.doi.org/10.1021/ja507822j | J. Am. Chem. Soc. 2014, 136, 16240–16250

paralogs which could use different routes as a function of the growth conditions, being the choice of one route over the other dictated by (i) intrinsic features of the apo target, such as stability of its Fe/S cluster and its cellular concentration, (ii) its affinity toward components of the Fe/S cluster biosynthesis system, and (iii) the overall cellular demand for Fe/S clusters under given conditions. These aspects are, however, not maintained in more evolved organisms such as yeast and humans, which contain indeed only two A-type proteins (ISCA1 and ISCA2 in humans and Isa1 and Isa2 in yeast) that are not functionally redundant.[20,52] Both proteins are essential for the generation of [4Fe-4S] clusters, interacting each other for this function.[6−8] Nevertheless, how these two A-type proteins operate in molecular terms to generate [4Fe-4S] clusters was not yet defined. To address this aspect, in this work we have (i) structurally characterized human ISCA2 and its Fe/S binding properties; (ii) investigated the protein−protein interaction between hISCA2 and hISCA1; (iii) addressed the cluster transfer and assembly on hISCA1/hISCA2 by the addition of the protein partner $[2Fe\text{-}2S]^{2+}$ hGRX5.

The structural studies on apo hISCA2 support a model wherein the protein has a dimeric structural organization similar to that found for the bacterial homologue *E. coli* SufA.[22] In its dimeric state, the subunit−subunit interface exhibits backbone dynamic motions indicative of an intrinsic propensity for the subunit to be swapped with other protein partners. This aspect is confirmed by protein−protein interaction studies with apo hISCA1, which showed indeed that apo hISCA2 switches from a homodimer to a heterodimer involving, as interacting interface, the same protein surface involved in the subunit−subunit contacts of homodimeric apo hISCA2. We provided therefore clear evidence that apo hISCA1 and apo hISCA2 associate each other to form a heterodimer whose formation is favored with respect to the monomeric and/or homodimeric states of hISCA1 and hISCA2. hISCA2 is able to bind, upon chemical reconstitution, a [4Fe-4S] cluster in a dimeric state undergoing only local structural rearrangements at the dimeric interface. 1D ^{1}H paramagnetic NMR spectra of chemically reconstituted hISCA2 indicate the presence of three $[4Fe\text{-}4S]^{+}$ bound species, whose relative ratios largely depends by the chemical reconstitution. The observed chemical speciation might be the result of the dynamic processes detected at the protein−protein interface, which do not stabilize a unique conformation or iron coordination. The obtainment of these species, however, shows that dimeric hISCA2 is able to bind a [4Fe-4S] cluster, which can be assembled, as suggested by ESI-MS data, in a stepwise process converting a [2Fe-2S] cluster-bound form into a [4Fe-4S] cluster-bound form. However, given that hISCA2 homodimer switches to the heterodimer upon addition of hISCA1 and that this heterodimer is also able to bind a [4Fe-4S] cluster upon chemical reconstitution, the heterodimer should be considered as the physiologically relevant species for assembling [4Fe-4S] clusters in vivo.

Recently, we found that both hISCA1 and hISCA2 proteins can individually receive a $[2Fe\text{-}2S]^{2+}$ cluster from its physiological partner $[2Fe\text{-}2S]^{2+}$ hGRX5 through the formation of a cluster-mediated, low-populated protein−protein adduct.[27] The same mechanism, i.e., a cluster transfer without the permanent formation of a ternary hGRX5/hISCA1/hISCA2 complex, is also observed when $[2Fe\text{-}2S]^{2+}$ hGRX5 was mixed with the apo hISCA1/hISCA2 complex. On the other hand, when $[2Fe\text{-}2S]^{2+}$ hGRX5 is added to the individual proteins, a $[2Fe\text{-}2S]^{2+}$ cluster-bound species of hISCA1 and hISCA2 is obtained as a product,[27] whereas a $[4Fe\text{-}4S]^{2+}$ cluster is assembled on the heterodimeric hISCA2/hISCA1 complex upon incubation with 2 equiv of $[2Fe\text{-}2S]^{2+}$ hGRX5. Therefore, the heterodimeric complex acts as the "assembler" of [4Fe-4S] clusters; i.e., the two hGRX5-donated $[2Fe\text{-}2S]^{2+}$ clusters generate a $[4Fe\text{-}4S]^{2+}$ cluster on the preformed heterodimeric complex. Since we showed that hISCA2 can bind both [2Fe-2S] and [4Fe-4S] clusters in a dimeric state and that these species can interconvert each other, a [2Fe-2S] cluster bound form might be therefore the reaction intermediate required to form the [4Fe-4S] cluster in the hISCA1/hISCA2 complex. The formation of the same $[4Fe\text{-}4S]^{2+}$ cluster-bound heterodimeric species is also observed by preforming $[2Fe\text{-}2S]^{2+}$ hISCA2 and $[2Fe\text{-}2S]^{2+}$ hISCA1, and then mixing them together. In such a case, hISCA1 and hISCA2 independently receive the $[2Fe\text{-}2S]^{2+}$ cluster from hGRX5 and then form the heterodimeric $[4Fe\text{-}4S]^{2+}$ cluster-bound complex. Again, these data support a functional role of the heterodimeric hISCA2/hISCA1 complex in assembling $[4Fe\text{-}4S]^{2+}$ clusters. In both possible $[4Fe\text{-}4S]^{2+}$ assembly mechanism scenarios, a coupling of two $[2Fe\text{-}2S]^{2+}$ clusters is required to generate a $[4Fe\text{-}4S]^{2+}$ cluster. The reductive coupling process of two $[2Fe\text{-}2S]^{2+}$ clusters to form a single $[4Fe\text{-}4S]^{2+}$ cluster is already well described in the literature on the bacterial proteins IscU[53,54] and IscA.[15] In these cases, a $[4Fe\text{-}4S]^{2+}$ cluster per homodimer is assembled via species containing one or two $[2Fe\text{-}2S]^{2+}$ cluster(s) per homodimer. Similarly, SufA was found to be capable to mature [4Fe-4S] target enzymes.[55,56] However, such studies did not show whether the reductive coupling of two $[2Fe\text{-}2S]^{2+}$ clusters occurs on SufA prior to cluster transfer or on the target protein after transfer. A reducing agent was absolutely required in the described reductive coupling processes, as expected for a reaction converting ferric ions present in $[2Fe\text{-}2S]^{2+}$ clusters into a mixture of ferric and ferrous ions in $[4Fe\text{-}4S]^{2+}$ clusters. In bacterial IscU, SufA and IscA, dithionite and DTT were the electron donors.[15,53−55] It is reasonable that the two $[2Fe\text{-}2S]^{2+}$ clusters transferred from hGRX5 to its protein partners hISCA1 and hISCA2,[57,58] isolated or in a complex already, assemble a $[4Fe\text{-}4S]^{2+}$ cluster by a reductive coupling process. This process is active only once the heterodimeric complex is formed as hISCA1 and hISCA2 are unable individually to form a $[4Fe\text{-}4S]^{2+}$ cluster species once receiving the $[2Fe\text{-}2S]^{2+}$ clusters from hGRX5. DTT and/or GSH molecules, which are present in excess in all protein mixtures, are the best candidates to act as reducing agents toward the heterodimeric complex.

Considering that eukaryotic ISCA1 and ISCA2 are found as a complex in the cells,[6] our data support a model where the function of the heterodimeric complex in eukaryotes is that of assembling [4Fe-4S] clusters required for maturation of mitochondrial [4Fe-4S] target proteins. Since the activities of mitochondrial [4Fe-4S] target proteins, such as aconitase, were significantly diminished by depletion of either ISCA1 or ISCA2 proteins,[8] the here characterized [4Fe-4S] heterodimeric complex might thus be involved in the [4Fe-4S] transfer process to the [4Fe-4S] mitochondrial enzymes. However, the physiological electron donor in vivo still remains to be established. From our data we can suggest that IBA57, which is part of the in vivo detected complex,[9] might not have a crucial role in the reductive coupling reaction, since we showed that [4Fe-4S] clusters can be assembled on a hISCA1/hISCA2 complex lacking IBA57. This is in agreement with what already proposed on the molecular function of IBA57, i.e., that it

mediates the iron/iron−sulfur cluster transfer to target proteins[6] while it is not required for iron binding to the ISCA proteins.[9]

■ ASSOCIATED CONTENT

Supporting Information

Three figures reporting temperature dependence of hyperfine-shifted signals, ESI-MS spectra, paramagnetic 1D ^{1}H and diamagnetic $^{1}H-^{15}N$ HSQC NMR spectra, chemical shifts of apo hISCA2, pdb coordinates of the docking model of apo hISCA2, and a table reporting the scoring parameters of the docking model. This material is available free of charge via the Internet at http://pubs.acs.org.

■ AUTHOR INFORMATION

Corresponding Author

banci@cerm.unifi.it

Notes

The authors declare no competing financial interest.

■ ACKNOWLEDGMENTS

This work was supported by Bio-NMR (European FP7 Grant 261863), Ente Cassa di Risparmio, institutional research funding IUT (Grant IUT 19-8) of the Estonian Ministry of Education and Research, Estonian Science Foundation Grant No. 8811. This work was also supported by the European Integrated Structural Biology Infrastructure (INSTRUCT), which is part of the European Strategy Forum on Research Infrastructures and supported by national member subscriptions.

■ REFERENCES

(1) Lill, R.; Hoffmann, B.; Molik, S.; Pierik, A. J.; Rietzschel, N.; Stehling, O.; Uzarska, M. A.; Webert, H.; Wilbrecht, C.; Muhlenhoff, U. *Biochim. Biophys. Acta* **2012**, *1823*, 1491.

(2) Stehling, O.; Lill, R. *Cold Spring Harbor Perspect. Biol.* **2013**, *5*, a011312.

(3) Garland, S. A.; Hoff, K.; Vickery, L. E.; Culotta, V. C. *J. Mol. Biol.* **1999**, *294*, 897.

(4) Tong, W. H.; Rouault, T. A. *Cell Metab.* **2006**, *3*, 199.

(5) Muhlenhoff, U.; Gerber, J.; Richhardt, N.; Lill, R. *EMBO J.* **2003**, *22*, 4815.

(6) Muhlenhoff, U.; Richter, N.; Pines, O.; Pierik, A. J.; Lill, R. *J. Biol. Chem.* **2011**, *286*, 41205.

(7) Muhlenhoff, U.; Gerl, M. J.; Flauger, B.; Pirner, H. M.; Balser, S.; Richhardt, N.; Lill, R.; Stolz, J. *Eukaryotic Cell* **2007**, *6*, 495.

(8) Sheftel, A. D.; Wilbrecht, C.; Stehling, O.; Niggemeyer, B.; Elsasser, H. P.; Muhlenhoff, U.; Lill, R. *Mol. Biol. Cell* **2012**, *23*, 1157.

(9) Gelling, C.; Dawes, I. W.; Richhardt, N.; Lill, R.; Muhlenhoff, U. *Mol. Cell. Biol.* **2008**, *28*, 1851.

(10) Song, D.; Tu, Z.; Lee, F. S. *J. Biol. Chem.* **2009**, *284*, 35297.

(11) Long, S.; Changmai, P.; Tsaousis, A. D.; Skalicky, T.; Verner, Z.; Wen, Y. Z.; Roger, A. J.; Lukes, J. *Mol. Microbiol.* **2011**, *81*, 1403.

(12) Waller, J. C.; Alvarez, S.; Naponelli, V.; Lara-Nunez, A.; Blaby, I. K.; Da, S. V.; Ziemak, M. J.; Vickers, T. J.; Beverley, S. M.; Edison, A. S.; Rocca, J. R.; Gregory, J. F., III; Crecy-Lagard, V.; Hanson, A. D. *Proc. Natl. Acad. Sci. U. S. A.* **2010**, *107*, 10412.

(13) Ding, H.; Clark, R. J. *Biochem. J.* **2004**, *379*, 433.

(14) Mapolelo, D. T.; Zhang, B.; Naik, S. G.; Huynh, B. H.; Johnson, M. K. *Biochemistry* **2012**, *51*, 8056.

(15) Mapolelo, D. T.; Zhang, B.; Naik, S. G.; Huynh, B. H.; Johnson, M. K. *Biochemistry* **2012**, *51*, 8071.

(16) Morimoto, K.; Yamashita, E.; Kondou, Y.; Lee, S. J.; Arisaka, F.; Tsukihara, T.; Nakai, M. *J. Mol. Biol.* **2006**, *360*, 117.

(17) Krebs, C.; Agar, J. N.; Smith, A. D.; Frazzon, J.; Dean, D. R.; Huynh, B. H.; Johnson, M. K. *Biochemistry* **2001**, *40*, 14069.

(18) Wu, G.; Mansy, S. S.; Hemann, C.; Hille, R.; Surerus, K. K.; Cowan, J. A. *J. Biol. Inorg. Chem.* **2002**, *7*, 526.

(19) Jensen, L. T.; Culotta, V. C. *Mol. Cell. Biol.* **2000**, *20*, 3918.

(20) Kaut, A.; Lange, H.; Diekert, K.; Kispal, G.; Lill, R. *J. Biol. Chem.* **2000**, *275*, 15955.

(21) Bilder, P. W.; Ding, H.; Newcomer, M. E. *Biochemistry* **2004**, *43*, 133.

(22) Wada, K.; Hasegawa, Y.; Gong, Z.; Minami, Y.; Fukuyama, K.; Takahashi, Y. *FEBS Lett.* **2005**, *579*, 6543.

(23) Xu, D.; Liu, G.; Xiao, R.; Acton, T.; Goldsmith-Fischman, S.; Honig, B.; Montelione, G. T.; Szyperski, T. *Proteins* **2004**, *54*, 794.

(24) Cupp-Vickery, J. R.; Silberg, J. J.; Ta, D. T.; Vickery, L. E. *J. Mol. Biol.* **2004**, *338*, 127.

(25) Ollagnier-de-Choudens, S.; Mattioli, T.; Takahashi, Y.; Fontecave, M. *J. Biol. Chem.* **2001**, *276*, 22604.

(26) Uzarska, M. A.; Dutkiewicz, R.; Freibert, S. A.; Lill, R.; Muhlenhoff, U. *Mol. Biol. Cell* **2013**, *24*, 1830.

(27) Banci, L.; Brancaccio, D.; Ciofi-Baffoni, S.; Del Conte, R.; Gadepalli, R.; Mikolajczyk, M.; Neri, S.; Piccioli, M.; Winkelmann, J. *Proc. Natl. Acad. Sci. U. S. A.* **2014**, *111*, 6203.

(28) Keller, R. *The Computer Aided Resonance Assignment Tutorial*; CANTINA Verlag: Goldau, 2004; pp 1−81.

(29) Shen, Y.; Delaglio, F.; Cornilescu, G.; Bax, A. *J. Biomol. NMR* **2009**, *44*, 213.

(30) Luchinat, C.; Piccioli, M.; Pierattelli, R.; Engelke, F.; Marquardsen, T.; Ruin, R. *J. Magn. Reson.* **2001**, *150*, 161.

(31) Banci, L.; Bertini, I.; Ciurli, S.; Ferretti, S.; Luchinat, C.; Piccioli, M. *Biochemistry* **1993**, *32*, 9387.

(32) Banci, L.; Bertini, I.; Ciofi-Baffoni, S.; Boscaro, F.; Chatzi, A.; Mikolajczyk, M.; Tokatlidis, K.; Winkelmann, J. *Chem. Biol.* **2011**, *18*, 794.

(33) Siegel, L. M. *Anal. Biochem.* **1965**, *11*, 126.

(34) Shen, Y.; Lange, O.; Delaglio, F.; Rossi, P.; Aramini, J. M.; Liu, G.; Eletsky, A.; Wu, Y.; Singarapu, K. K.; Lemak, A.; Ignatchenko, A.; Arrowsmith, C. H.; Szyperski, T.; Montelione, G. T.; Baker, D.; Bax, A. *Proc. Natl. Acad. Sci. U. S. A.* **2008**, *105*, 4685.

(35) Sali, A.; Potterton, L.; Yuan, F.; Van Vlijmen, H.; Karplus, M. *Proteins Struct. Funct. Genet.* **1995**, *23*, 318.

(36) de Vries, S. J.; van Dijk, M.; Bonvin, A. M. *Nat. Protoc.* **2010**, *5*, 883.

(37) Wollenberg, M.; Berndt, C.; Bill, E.; Schwenn, J. D.; Seidler, A. *Eur. J. Biochem.* **2003**, *270*, 1662.

(38) Ding, H.; Clark, R. J.; Ding, B. *J. Biol. Chem.* **2004**, *279*, 37499.

(39) Roy, A.; Kucukural, A.; Zhang, Y. *Nat. Protoc.* **2010**, *5*, 725.

(40) Dominguez, C.; Boelens, R.; Bonvin, A. M. *J. Am. Chem. Soc.* **2003**, *125*, 1731.

(41) Landry, A. P.; Cheng, Z.; Ding, H. *Dalton Trans.* **2013**, *42*, 3100.

(42) Phillips, W. D.; McDonald, C. C.; Stombaugh, N. A.; Orme-Johnson, W. H. *Proc. Natl. Acad. Sci. U. S. A.* **1974**, *71*, 140.

(43) Bertini, I.; Capozzi, F.; Luchinat, C.; Piccioli, M.; Vila, A. J. *J. Am. Chem. Soc.* **1994**, *116*, 651.

(44) Banci, L.; Ciofi-Baffoni, S.; Mikolajczyk, M.; Winkelmann, J.; Bill, E.; Eirini Pandelia, M. *J. Biol. Inorg. Chem.* **2013**, *18*, 883.

(45) Blondin, G.; Girerd, J.-J. *Chem. Rev.* **1990**, *90*, 1359.

(46) Bertini, I.; Capozzi, F.; Ciurli, S.; Luchinat, C.; Messori, L.; Piccioli, M. *J. Am. Chem. Soc.* **1992**, *114*, 3332.

(47) Bertini, I.; Briganti, F.; Luchinat, C.; Messori, L.; Monnanni, R.; Scozzafava, A.; Vallini, G. *Eur. J. Biochem.* **1992**, *204*, 831.

(48) Malkin, R.; Rabinowitz, J. C. *Biochem. Biophys. Res. Commun.* **1966**, *23*, 822.

(49) Johnson, D. C.; Dean, D. R.; Smith, A. D.; Johnson, M. K. *Annu. Rev. Biochem.* **2005**, *74*, 247.

(50) Roche, B.; Aussel, L.; Ezraty, B.; Mandin, P.; Py, B.; Barras, F. *Biochim. Biophys. Acta* **2013**, *1827*, 455.

(51) Lill, R. *Nature* **2009**, *460*, 831.

(52) Pelzer, W.; Muhlenhoff, U.; Diekert, K.; Siegmund, K.; Kispal, G.; Lill, R. *FEBS Lett.* **2000**, *476*, 134.

(53) Chandramouli, K.; Unciuleac, M. C.; Naik, S.; Dean, D. R.; Huynh, B. H.; Johnson, M. K. *Biochemistry* **2007**, *46*, 6804.
(54) Agar, J. N.; Krebs, C.; Frazzon, J.; Huynh, B. H.; Dean, D. R.; Johnson, M. K. *Biochemistry* **2000**, *39*, 7856.
(55) Gupta, V.; Sendra, M.; Naik, S. G.; Chahal, H. K.; Huynh, B. H.; Outten, F. W.; Fontecave, M.; Ollagnier, d. C *J. Am. Chem. Soc.* **2009**, *131*, 6149.
(56) Ollagnier-de-Choudens, S.; Sanakis, Y.; Fontecave, M. *J. Biol. Inorg. Chem.* **2004**, *9*, 828.
(57) Vilella, F.; Alves, R.; Rodriguez-Manzaneque, M. T.; Belli, G.; Swaminathan, S.; Sunnerhagen, P.; Herrero, E. *Comp. Funct. Genomics* **2004**, *5*, 328.
(58) Kim, K. D.; Chung, W. H.; Kim, H. J.; Lee, K. C.; Roe, J. H. *Biochem. Biophys. Res. Commun.* **2010**, *392*, 467.